

Article

Not peer-reviewed version

Aerosol Longwave Radiative Forcing in the Arctic: Forty Years of Change Under Reducing Global SO₂ Emissions

[Andrey Zachek](#)* and [Leonid Yurganov](#)

Posted Date: 27 February 2026

doi: 10.20944/preprints202602.1778.v1

Keywords: arctic aerosols; longwave radiation; arctic haze; sulfur dioxide emissions



Preprints.org is a free multidisciplinary platform providing preprint service that is dedicated to making early versions of research outputs permanently available and citable. Preprints posted at Preprints.org appear in Web of Science, Crossref, Google Scholar, Scilit, Europe PMC.

Copyright: This open access article is published under a [Creative Commons CC BY 4.0 license](#), which permit the free download, distribution, and reuse, provided that the author and preprint are cited in any reuse.

Disclaimer/Publisher's Note: The statements, opinions, and data contained in all publications are solely those of the individual author(s) and contributor(s) and not of MDPI and/or the editor(s). MDPI and/or the editor(s) disclaim responsibility for any injury to people or property resulting from any ideas, methods, instructions, or products referred to in the content.

Article

Aerosol Longwave Radiative Forcing in the Arctic: Forty Years of Change Under Reducing Global SO₂ Emissions

Andrey Zachek ^{1,2,*} and Leonid Yurganov ³

¹ Sulam Tsor High School, Gesher HaZiv 2281500, Israel

² Arctic and Antarctic Research Institute (AARI), 38 Bering str., St. Petersburg 199397, Russia

³ Independent Researcher, USA

* Correspondence: 1zachek@gmail.com

Abstract

This study presents a comprehensive assessment of the longwave radiative effects of Arctic tropospheric aerosols based on unique measurements collected at the North Pole drifting station SP-28 in 1987. The primary objective is to compare these historical observations with modern datasets from the Surface Heat Budget of the Arctic Ocean (SHEBA, 1997–1998) and the Multidisciplinary drifting Observatory for the Study of Arctic Climate (MOSAiC, 2019–2020) to evaluate long-term changes in the Arctic radiation regime. Continuous longwave radiation measurements were obtained using high-precision spectral pyrgeometers, and a new diagnostic approach was introduced that employs the standard deviation of longwave radiation together with the normalized longwave aerosol effect (NLAE) to identify haze inversion layers. The results show that in 1987, sub-inversion haze layers enhanced the downward longwave flux by 15–20 W/m² and increased atmospheric emissivity. In contrast, MOSAiC observations reveal emissivity values that closely match aerosol-free model calculations, indicating a substantial decline in Arctic haze and the disappearance of radiatively significant aerosol layers. This shift is consistent with the long-term reduction of sulfur dioxide emissions across the Northern Hemisphere and suggests that gaseous components now dominate the formation of inversion radiative properties in the modern Arctic.

Keywords: arctic aerosols; longwave radiation; arctic haze; sulfur dioxide emissions

1. Introduction

Radiative heat transfer between the atmosphere and the surface is a fundamental component of the Earth's energy balance and plays a central role in shaping the thermal structure of the lower troposphere. Even small variations in the concentration of radiatively active gases or aerosols can significantly modify longwave fluxes and influence the stability of the surface layer, especially in the Arctic, where strong temperature inversions and limited solar input amplify these effects.

Although the Arctic atmosphere has traditionally been regarded as exceptionally clean, observations beginning in the mid-20th century revealed that substantial amounts of anthropogenic aerosol are transported into the region during winter and spring from mid-latitude industrial areas of Eurasia and North America [1,2]. These pollutants form a persistent sub-inversion haze—one of the defining features of Arctic haze—which affects both shortwave and longwave radiative transfer. However, for many years the longwave radiative impact of this haze remained poorly quantified due to the lack of high-precision measurements.

Modern observations show that the radiation regime of the Arctic has undergone significant changes over the past 25–30 years. The 1987 data of SP-28 [3], SHEBA [4] and MOSAiC [5] were the observational basis that allowed the authors to obtain a unique long-term series demonstrating a

gradual weakening of the aerosol effect on longwave radiation, the authors obtained a unique long-term series demonstrating a gradual weakening of the aerosol effect on longwave radiation.

A clear visual manifestation of this phenomenon is shown in Figure 1, which illustrates the appearance and vertical structure of Arctic haze under different observational conditions. These images, obtained by the author during flights in the North Pole region, demonstrate the stratified nature of the aerosol layer and its persistence within strong surface inversions. Such visual evidence supports earlier theoretical and experimental studies that emphasized the ability of thin aerosol layers to exert a measurable longwave radiative effect even at very low optical thickness.

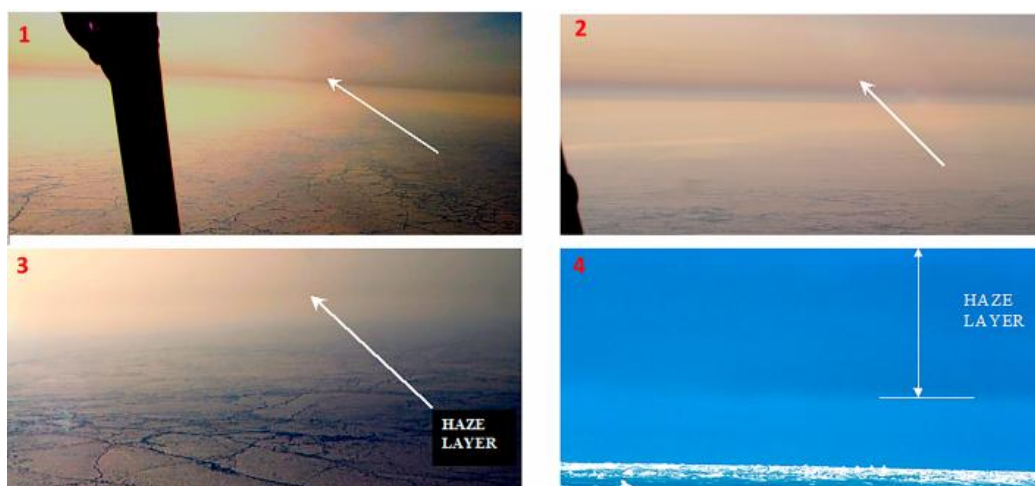


Figure 1. Visual observations of Arctic haze at different altitudes.

During flights conducted on 17–19 April 2001, photographs of the haze layer were obtained at altitudes of 350 m, 400 m, and 180 m, as well as from the surface of sea ice. Panels 1–3 show the haze as observed from aircraft at different heights, while panel 4 presents the view from the ice surface.

The first continuous longwave radiation measurements capable of resolving the radiative signature of sub-inversion haze was obtained at the drifting station SP-28 in 1987. These observations demonstrated that aerosol-condensation layers located within strong surface inversions can substantially enhance downward longwave radiation and increase atmospheric emissivity. The term “atmospheric emissivity” is explained in the section 2.6.

Measurements in the late 1980s confirmed the magnitude of this effect, indicating that radiatively active aerosol layers were a persistent element of the Arctic atmosphere at that time.

The physical mechanisms underlying this enhancement were consistent with earlier theoretical developments. Wexler [6] first described the formation of strong surface inversions in polar air masses, while Curry [7] later showed that even small amounts of condensate within an inversion can dramatically increase longwave cooling efficiency. Additional studies in the 1980s and early 1990s [8–10] demonstrated that thin aerosol or condensation layers embedded within stable inversions can exert a disproportionately strong influence on longwave fluxes.

Over the past several decades, however, the Arctic radiation regime has undergone substantial changes. Reanalysis of SP-28 data, combined with newly processed observations from the SHEBA [4] and the MOSAiC [5], reveals a systematic decline in the longwave aerosol effect. Modern emissivity values closely match calculations for an aerosol-free atmosphere, suggesting that radiatively significant sub-inversion haze has largely disappeared. This shift coincides with a long-term reduction in anthropogenic sulfur dioxide emissions across the Northern Hemisphere, which has led to a pronounced decrease in sulfate aerosol—the primary component of Arctic haze.

The aim of this study is to quantify the longwave radiative impact of Arctic haze using historical and modern datasets and to assess how the decline in anthropogenic sulfur emissions has altered the radiative properties of the Arctic atmosphere over the past four decades.

2. Methods and Materials

Experimental studies were carried out at the drifting station SP-28, which operated in the Central Polar Basin from February to October 1987.

2.1. Mode and Experimental Setup

The drift area covered latitudes of 81–85° N and longitudes of 140–170° E, which corresponded to one of the most remote and climatically stable regions of the Arctic. These conditions ensured minimal influence of local aerosol sources and allow us to consider the observed radiation characteristics as a reflection of large-scale processes of transport and transformation of air masses.

The station was located on multiyear sea ice several meters thick, which provided a stable platform for the installation of radiation instruments as shown in Figure 2. The absence of open water in the drift zone eliminated the influence of local thermal anomalies and ensured the homogeneity of the underlying surface, which is an important condition for the correct interpretation of longwave measurements.



Figure 2. Radiation measurement site of the SP-28 drifting station.

The Central Polar Basin is characterized by a long period of polar night, abrupt seasonal changes in temperature, and sustained surface inversions, making it an ideal natural laboratory for studying longwave radiation exchange and the effects of sub-inversion haze. The spring, when the peak aerosol transport from the middle latitudes is observed, is especially important for the analysis of the seasonal evolution of atmospheric radiation parameters.

The synoptic situation in the Arctic in the first half of 1987, as illustrated in Figure 3, created unique conditions for the study of the longwave radiation effects of aerosol. During the entire observation period at SP-28, a pronounced anticyclonic regime prevailed, accompanied by increased background pressure and stable surface subinversion, key elements contributing to the accumulation of aerosol in the lower troposphere.

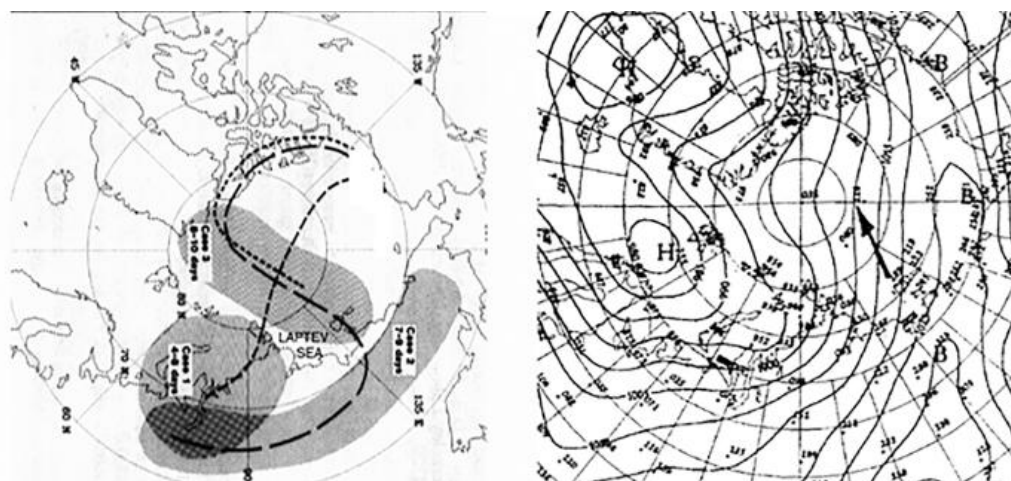


Figure 3. Synoptic circulation and aerosol transport during the SP-28 observation period.

The average monthly pressure in the drift area exceeded the climatological norm by 4–6 hPa, which indicated an abnormally strong Arctic anticyclone system. The air temperature in January–March was 2–7 °C below normal, and in April–June it was near to the average. Such conditions contributed to the formation of strong surface subinversion, which play a central role in retaining the sub-inversion haze and enhancing its longwave impact.

During the period from February 18 to April 4, the drift area was in the zone of interaction between North Atlantic cyclones and the eastern periphery of the Arctic anticyclone. During this period, the wind was mainly southwesterly, which created favorable conditions for the transfer of aerosol from the industrial regions of Siberia, including the Norilsk industrial area. These features are consistent with known seasonal patterns of impurity transport in the Siberian sector of the Arctic, described in international studies. From April 5 to June 24, a stable anticyclonic regime was established with easterly winds and pressure 4–6 hPa above normal. During this period, the strongest inversions and the maximum probability of subinversion haze formation were observed. It was during these months that the most pronounced anomalies of longwave radiation associated with the aerosol condensation layer were recorded.

Thus, the synoptic conditions of 1987 provided a favorable background for studying the Arctic haze longwave effects: sustained inversions, weak turbulence, lack of precipitation, and long periods of cloudless skies.

2.2. Radiometric Equipment

For precise measurements of downwelling longwave radiation, spectral pyrgeometers P2-30 (1.8–30 μm) and P8-12 (8–12 μm) were used in the development of the ideas laid down by Hinzpeter, H. [11]. These instruments, developed at the Arctic and Antarctic Research Institute (AARI) by Zachek A. [12] through deep modernization balance meter created at the Main Geophysical Observatory (MGO) by Zachek S., [13], are shown in Figure 4.

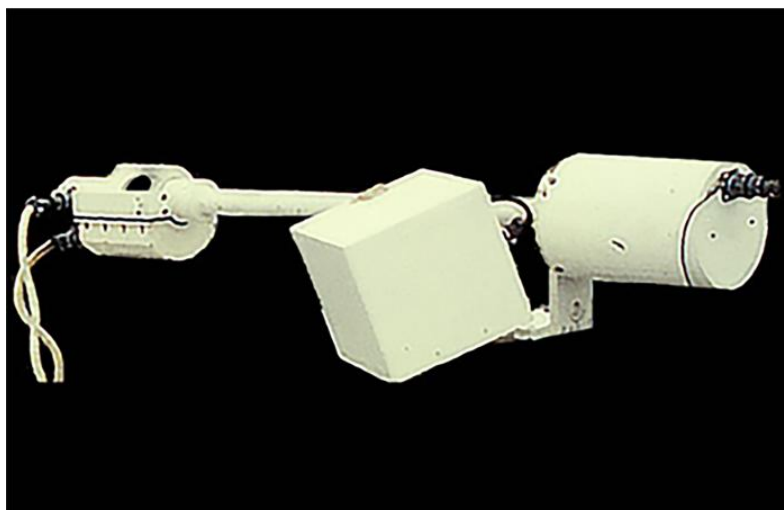


Figure 4. Pyrgeometer P2-30 (1.8–30 μm).

The devices are equipped with highly sensitive MTS-P thermoelectric receivers, built-in controllable hollow-cavity blackbody emitters, and flat germanium filters installed in a dynamic modulator stage.

The use of flat optics in combination with a balanced differential measurement scheme makes it possible not only to achieve the international standards accuracy, such as Kipp & Zonen CGR4 [14], but also to surpass them in a number of critical parameters. Under conditions of high azimuthal isotropy of atmospheric radiation at zenith angles $>50^\circ$, the flat filter eliminates the complex optical distortions and parasitic reflections characteristic of meniscus domes. The key advantage of the design is the implementation of the principle of “dynamic indifference” to its own thermal background: thanks to the methodological control phase, any temperature gradients of moving parts are fully compensated by the balance scheme. In contrast to classical pyrgeometers, which require complex mathematical corrections for the “window heating offset” Gröbner, J., & Wacker, S. [15], the P2-30 device provides physical subtraction of parasitic signals. This made it possible to integrate an active heating system for the internal volume (heated by $+10^\circ$) for reliable protection against hydrometeors.

The instruments operating in the extreme conditions of Arctic drifting stations and Antarctic expeditions demonstrated their unique stability. Under the same conditions, meniscus-dome systems from Eppley and Kipp & Zonen exhibited significant distortions caused by dome icing, as reported by Riihelä et al. (2020) [16]. The presence of the “dual temperature” mode of the reference emitter makes the device function as an autonomous reference standard, providing continuous sensitivity verification directly during the monitoring process. Field comparisons reported by König-Langlo and Zachek [17], including joint measurements with the Eppley pyrgeometer, showed that the P2-30 remained stable even under heavy icing, whereas the Eppley instrument exhibited significant distortion (Figure 5).

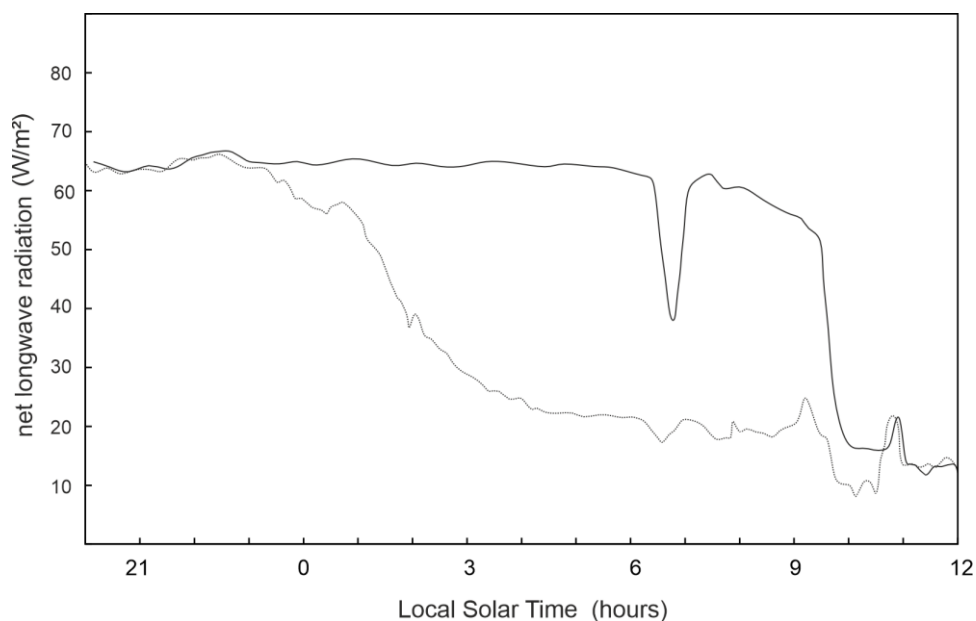


Figure 5. Field comparison results.

Figure 5 shows that during the icing event that began at 23:00 local solar time on 2 October 1989 in the Weddell Sea, the P2-30 maintained a stable signal (solid line), whereas the Eppley pyrgeometer exhibited pronounced distortion under the same conditions (dotted line).

This confirms the unique suitability of AARI instruments for operation in polar night conditions.

2.3. Cloud Boundary and Vertical Visibility

The lower boundary of the cloud cover was determined using the IMO1 pulsed-light locator, which allowed thin stratus clouds that are not visually distinguishable to be excluded from the analysis.

2.4. Aerological Data

For the calculation of longwave radiation, aerological sounding data obtained with the D22 “Malachite” radio-theodolite system (Zaitseva [18]) were used. Temperature, humidity, and pressure profiles served as input parameters for the Shechter radiative-transfer model [14], which was used to calculate longwave radiation in an aerosol-free atmosphere.

2.5. Method of Sub-Inversion Haze Extraction

There are no visual and instrumental methods for observing sub-inversion haze, and the existing measuring instruments did not have sufficient sensitivity. Therefore, the most promising way to detect such haze is to analyze the temporal evolution of longwave radiation in the atmosphere, using an approach similar to variability-based cloud-identification methods. To classify radiation conditions, the variability characteristics of time series of longwave radiation were used. The diagnostic parameter was the standard deviation (RMS), calculated for each hourly interval as the deviation of instantaneous values from the mean for that hour. This approach allowed the level of radiation-field variability to be quantified and related to the physical states of the atmosphere. LWnet fluctuations can be used as a diagnostic indicator of Arctic haze.

Figure 6 illustrates the fluctuations of LWnet (curve 1) and its low-frequency trend (dotted line) during different stages of sub-inversion haze development (a–e). Analysis of these fluctuations showed that each atmospheric state corresponds to a characteristic RMS range.

Under cloud-free conditions, the RMS is below 0.1 W/m^2 , reflecting the high stability of the radiative background (a). For clear skies without haze, the RMS is on the order of 0.1 W/m^2 , indicating an almost complete absence of aerosol-induced disturbances (b).

During the presence and intensification of haze, the RMS increases to $0.2\text{--}0.7 \text{ W/m}^2$, which signifies growing aerosol optical thickness and enhanced small-scale variability (c). When the haze transitions into a stratus layer, the RMS exceeds 2 W/m^2 , indicating the formation of a stratus cloud deck and a pronounced rise in radiative instability (d).

This criterion allowed the observations to be reliably classified according to atmospheric conditions and ensured the consistency of subsequent radiation calculations. Weather conditions during the observation period remained stable: there was no frontal activity, no advection of new aerosol masses, and no change in the concentration of condensation nuclei. At about 18:00, the Sun went below the horizon, which led to a gradual radiative cooling of the surface layer of the Arctic haze. With the concentration of condensation nuclei remaining steady, microphysical transformations occurred: microdroplets and microcrystals grew in size due to water-vapor redistribution and local thermodynamic effects.

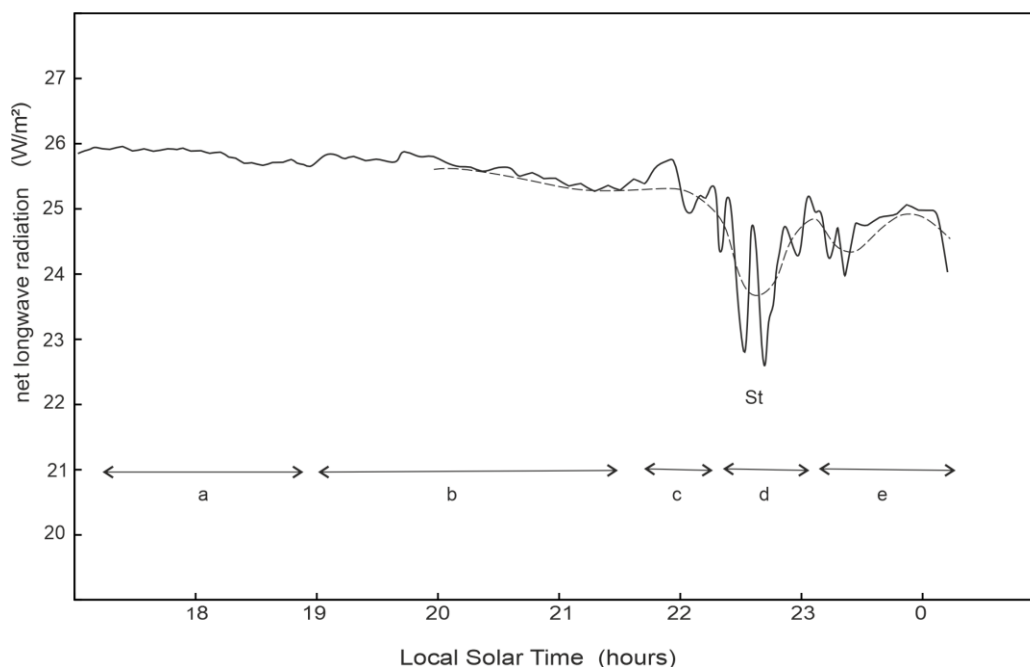


Figure 6. Fluctuations net longwave radiation during sub-inversion haze evolution.

The ceilometer detected the emergence of a backscattered signal at altitudes of 140–180 m (period d), and simultaneous longwave-radiation measurements with the P-2-30 pyrgeometer showed an increase in the standard deviation of LWnet, despite the aerosol concentration remaining unchanged.

Thus, the transitional regime did not result from changes in particle concentration but from the internal microphysical evolution of the layer under evening cooling.

Figure 6 presents the variability of net longwave radiation (solid line) and its spectral-frequency trend (dotted line) during stages (a–e) of Arctic haze development on 19 March 1997.

During the transition from haze to cloudiness, the surface LWnet changes only slightly (about 4 W/m^2).

This suggests that aerosol particles became hydrated during the haze phase, and the enhanced radiative effect resulted from condensational and sublimational growth. Recent studies [19] support this interpretation.

2.6. Approach to Determining the Aerosol Effect

The aerosol effect on the components of the atmospheric radiative balance is evaluated by comparing measured and calculated longwave-radiation characteristics. The key parameter in this comparison is the atmospheric emissivity, which represents an integrated measure of the atmosphere's longwave-emission efficiency.

The calculated emissivity (ϵ_{calc}) is a dimensionless quantity obtained from the Shekhter radiative-transfer model [20], which accounts only for the gaseous constituents of the atmosphere (water vapor, CO_2 , O_3 , etc.) and the actual temperature profile. Aerosol contributions are not included in this calculation.

To characterize the radiative properties of the real atmosphere, the observed emissivity (ϵ_{obs}) was used. This dimensionless parameter describes the thermal-emission efficiency of the atmospheric column and is derived from direct measurements using the Stefan–Boltzmann law:

$$\epsilon_{\text{obs}} = \text{LWD} / \sigma \cdot T_a^4,$$

where LWD is the downward longwave radiation measured at the surface (W m^{-2}), σ is the Stefan–Boltzmann constant ($5.67 \times 10^{-8} \text{ W m}^{-2} \text{ K}^{-4}$), and T_a is the near-surface air temperature (K).

In contrast to the calculated (parameterized) values of ϵ_{calc} , which account only for gaseous absorption, the observed emissivity ϵ_{obs} incorporates the combined contribution of all radiatively active components in the sub-inversion layer. These include the intrinsic emission of water vapor and trace gases, the longwave radiation of aerosol formations (sub-inversion haze), and the contribution of fine condensation layers and ice crystals such as fogs and hazes.

Thus, the difference between ϵ_{obs} and ϵ_{calc} isolates the net radiative effect of aerosol and microphysical processes in the longwave range.

2.6.1. Physical Meaning of Comparing Calculated and Measured Parameters

If ϵ_{obs} exceeds ϵ_{calc} , this indicates the presence of an additional radiating layer in the atmosphere that is not represented in the gas-only model. The difference $\epsilon_{\text{obs}} - \epsilon_{\text{calc}}$ therefore quantifies the net aerosol contribution to longwave radiation.

However, the absolute value of $\epsilon_{\text{obs}} - \epsilon_{\text{calc}}$ depends on the temperature and structure of the surface inversion, which complicates comparisons between different seasons and field campaigns. A parameter is therefore required that

- eliminates temperature dependence,
- isolates only the aerosol contribution,
- has a strict zero limit in aerosol-free conditions,
- remains dimensionless and universally applicable.

These requirements are met by the normalized longwave aerosol effect (NLAE), defined as

$$\text{NLAE} = \epsilon_{\text{obs}} - \epsilon_{\text{calc}}.$$

This normalized difference between the observed and calculated (aerosol-free) longwave flux serves as a strict indicator of aerosol influence.

2.6.2. Practical Necessity of NLAE

Obtaining reliable values requires identifying cloud-free periods. However, in polar regions cloud detection is difficult, especially during the polar night. Moreover, standard meteorological observations do not register sub-condensation haze unless it reaches the surface. Under such conditions, the comparison of ϵ_{obs} and ϵ_{calc} becomes particularly important, and NLAE is the only parameter that reliably isolates the aerosol contribution.

3. Results

The results are based on the SP-28 in situ observations and on the SHEBA and MOSAiC measurement data, which were processed and analyzed using the developed methodology.

3.1. Seasonal Evolution of Atmospheric Emissivity

The seasonal emissivity curves obtained from the SP28 (1987), SHEBA (1997–1998), and MOSAiC (2019–2020) datasets (Figure 7) exhibit a consistent multi-decadal transformation of the radiative state of the Arctic lower atmosphere.

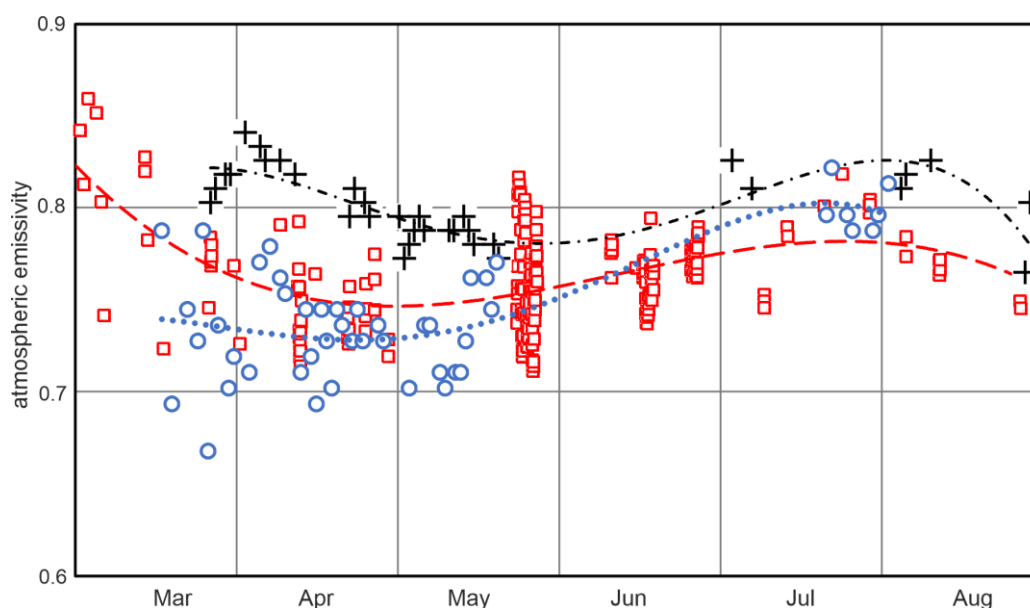


Figure 7. Seasonal variations in cloud-free atmospheric emissivity.

Each dataset is represented by a distinct marker and trend style: SP28 by black cross markers with a black dotted polynomial trend line, SHEBA by red square markers with a red dashed polynomial trend line, and MOSAiC by blue circular markers with a blue dotted polynomial trend line. These graphical distinctions allow the long-term evolution of emissivity to be traced clearly across the three expeditions.

A separate comparison is provided in Figure 8, where SP-28 emissivity is plotted using black square markers together with a black polynomial trend line representing the aerosol-free Shechter model. This figure highlights the magnitude of the aerosol contribution in 1987: throughout late winter and early spring, the SP-28 observations lie well above the model curve. The divergence between the black squares (observations) and the smooth polynomial model line quantifies the longwave enhancement produced by the sub-inversion haze. The fact that the model trend is smooth and monotonic, while the observational curve shows a pronounced early-spring peak, confirms that the additional emission originates from aerosol rather than from the gaseous atmosphere.

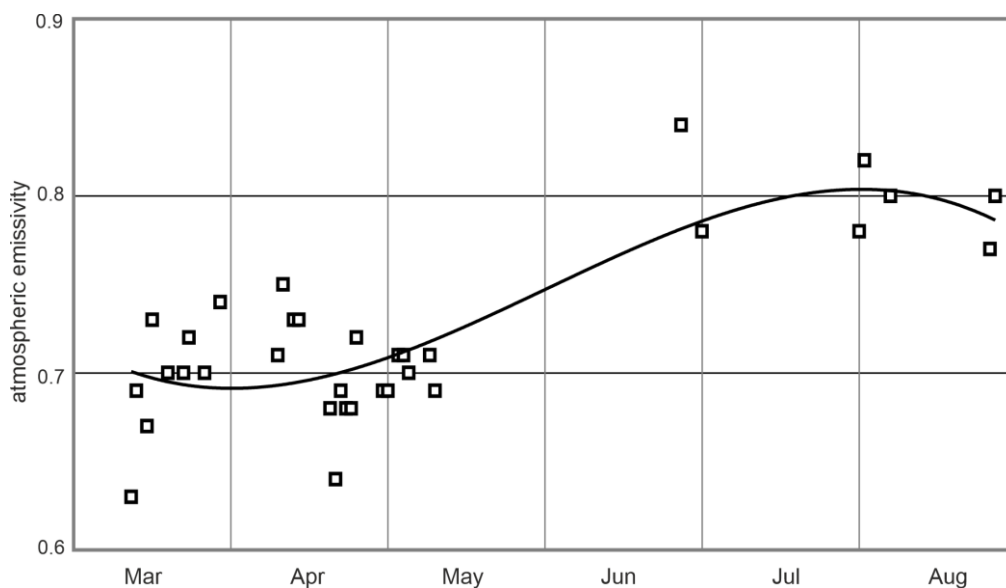


Figure 8. SP-28 emissivity compared with aerosol-free model calculations.

The SP-28 curve (1987) therefore shows the highest emissivity values during the transition season. The early-spring rise is steep and forms a pronounced first peak, reflecting the accumulation of sub-inversion haze, the strengthening of the aerosol–condensation layer, and the strong temperature inversion typical of the 1980s. During this period, ϵ_{obs} lies well above the aerosol-free Shechter model, indicating a substantial longwave contribution from aerosol. After this peak, the curve declines, forming a distinct spring minimum that marks the breakdown of the haze layer and the weakening of the inversion.

The SHEBA curve (1997–1998) occupies an intermediate position. The red square markers show a reduced early-spring peak compared to SP-28, and the red dashed polynomial trend line lies closer to the aerosol-free model. This indicates a transitional stage in which aerosol loading had already begun to decline, yet the haze layer still contributed measurably to longwave emission. The spring minimum becomes less pronounced, reflecting a partial shift from an aerosol-dominated to a gas-dominated radiative regime.

The MOSAiC curve (2019–2020), represented by blue circular markers and a blue dotted polynomial trend line, shows the lowest emissivity values among all expeditions. The early-spring peak is nearly absent, and the entire curve closely follows the aerosol-free model. This near-perfect agreement indicates that the modern Arctic atmosphere behaves radiatively as if it were aerosol-free. The disappearance of the aerosol-driven enhancement of ϵ_{obs} marks the collapse of the longwave-active haze layer. A detailed analysis of the seasonal curve shape reveals a bimodal structure with two physically distinct maxima. The first maximum, occurring in late winter to early spring, is sharp and associated with the presence of sub-inversion haze. Its steep rise reflects the rapid intensification of the aerosol–condensation layer and the strong temperature inversion. During this period, aerosol longwave emission becomes comparable to the gaseous contribution, producing a pronounced peak in ϵ_{obs} .

Following this peak, the curve declines into a spring saddle, which corresponds to the destruction of the haze layer, the weakening of the inversion, and the transition from an aerosol-dominated to a gas-dominated radiative regime.

The second maximum, observed in early summer, is smoother and driven primarily by the seasonal increase in water vapor, the rise in the optical thickness of the gaseous atmosphere, and the disappearance of the inversion. Unlike the first peak, this maximum is almost entirely controlled by water vapor.

Thus, the bimodal structure reflects two distinct radiative regimes:

- an aerosol-driven early-spring peak, and

- a water-vapor-driven summer peak.

The evolution from SP28 to SHEBA to MOSAiC demonstrates a clear long-term trend: the progressive weakening and eventual disappearance of the aerosol-driven peak, consistent with the decline in transported sulfate aerosol and the degradation of the Arctic haze.

3.2. Comparison of Observations with a Model Without Aerosol

Calculations of longwave radiation according to the Shekhter model performed for the temperature and humidity profiles SP-28 give a ϵ_{calc} curve that almost coincides with the MOSAiC observations (Figure 7). This means that:

- aerosol-free model,
- fully reproduces the modern atmosphere of the Arctic.

Such a coincidence would not have been possible in 1987, when the sub-inversion haze significantly increased ϵ_{obs} . Consequently, there is a degradation of Arctic haze associated with a long-term decrease in SO_2 emissions in the northern hemisphere.

3.3. Normalized Long Wave Aerosol Effect (NLAE)

NLAE values calculated for SP28 show a distinct seasonal maximum in March-April. This corresponds to the period of maximum transport of sulfate aerosol from mid-latitudes and the most developed sub-inversion haze.

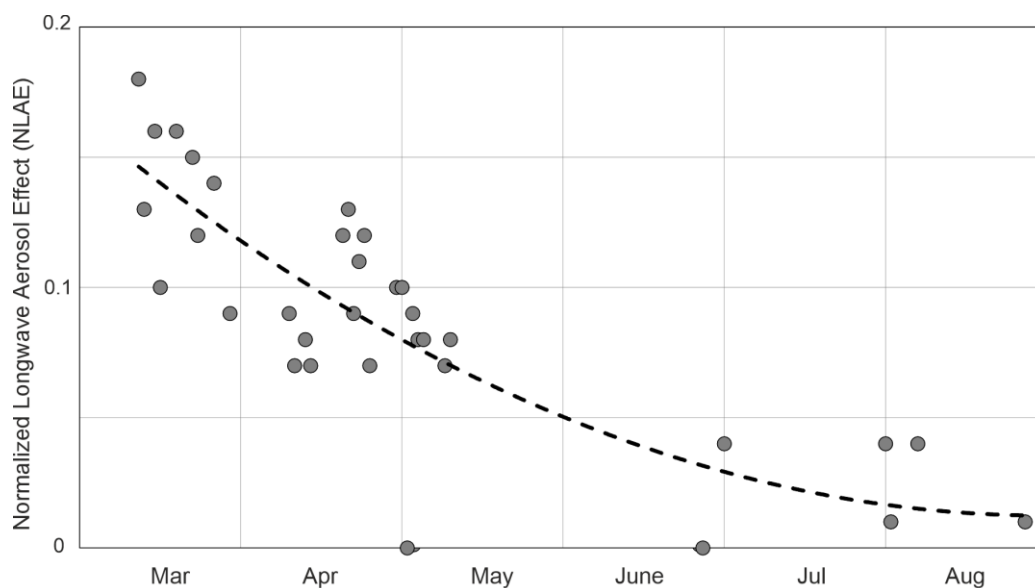


Figure 9. Seasonal course of the normalized longwave aerosol effect (NLAE) for SP-28.

Under MOSAiC, NLAE remains close to zero throughout the transition period. This means that:

- aerosol layer are absent,
- or its optical thickness is too small to have a noticeable longwave effect.

Thus, NLAE confirms the conclusions obtained from ϵ_{obs} : the modern Arctic is practically devoid of LW active aerosol.

3.4. Longwave Effect of Radiation Inversion

Under the conditions observed at SP-28, a surface-based temperature inversion containing an aerosol–condensation layer acted as the dominant source of longwave radiation. This structure enhanced:

- the downward longwave flux at the surface,
- the upward longwave flux at the top of the troposphere.

Consequently, such an inversion simultaneously:

- suppressed radiative cooling of the surface,
- intensified radiative cooling of the troposphere.

Under MOSAiC conditions, the inversion retains its structure, but its longwave effect is determined almost exclusively by the gaseous atmosphere, since the aerosol layer has disappeared.

4. Discussion

The presented results have formulated new research questions, identified relevant challenges, and outlined directions for further investigation.

4.1. Evolution of the Arctic Aerosol Regime over Time

Comparison of data from SP28 (1987), SHEBA (1997–1998) and MOSAiC (2019–2020) shows that the radiative properties of the Arctic atmosphere have undergone fundamental changes. The most important result is that the modern ϵ_{obs} curve is almost identical to the calculations of the Shechter radiative-transfer model for an aerosol-free atmosphere. Such agreement is possible only in the absence of a radiatively significant aerosol layer, which in the 1980s was a defining feature of Arctic haze.

This conclusion is consistent with the long-term decline in SO_2 emissions across the Arctic region, as documented by Crippa et al. [21]. Since sulfate aerosol was the dominant component of Arctic haze, the reduction in anthropogenic SO_2 emissions led to the degradation of the sub-inversion aerosol layer and the weakening of its longwave radiative impact. The magnitude and temporal structure of this decline are summarized in Table 1.

Table 1. Estimated Anthropogenic SO_2 Emissions in the Arctic Region (above 60°N), 1980–2020.

Year	$\text{SO}_2(\text{Mt/yr})$	Main Contributing Factors
1980	3.15	Peak of industrial activity; minimal emission controls.
1985	2.90	Initial implementation of regional air quality protocols.
1990	2.55	Industrial restructuring in the post-Soviet Arctic.
1995	2.20	Economic recession in major northern mining hubs.
2000	2.12	Stabilization of smelting operations in Norilsk.
2005	2.05	Start of local technological upgrades in metallurgy.
2010	1.88	Modernization of non-ferrous metal production.
2015	1.75	Phasing out of obsolete smelting capacities.
2020	1.52	Implementation of IMO 2020 (maritime fuel sulfur cap).

4.2. Changing the Role of Sub-Inversion Haze in Longwave Heat Transfer

During the North Pole-28 expedition (1987), the sub-inversion haze produced a pronounced increase in the downward longwave flux at the surface. The increment ΔLWD reached several W m^{-2} , substantially enhancing the integral emissivity of the atmosphere. The highest values of the NLAE parameter were observed in March–April, coinciding with the peak period of transboundary transport of anthropogenic pollutants from mid-latitudes.

In contrast, the modern MOSAiC data (2019–2020) indicate an almost complete absence of any aerosol contribution to longwave radiation in the central Arctic. Thus, the present-day radiative regime of the region is governed almost entirely by the gaseous composition of the atmosphere and by the temperature structure of the surface inversion.

A physical paradox arises from this process. The downward radiation increment ΔLWD recorded at the surface is equivalent to an increase in the total heat loss of the Earth–atmosphere system to space, because any additional downward emission is accompanied by an equal additional upward emission. As a result, the integral transmission function of the overlying layers in the infrared

transparency windows approaches unity ($P \approx 1$). Under these conditions, the upward longwave flux generated by the haze reaches the top of the atmosphere (TOA) almost without attenuation:

$$\Delta LWU_{TOA} \approx (\epsilon_{obs} - \epsilon_{calc}) \sigma T_{aer}^4,$$

where T_{aer} is the kinetic temperature of the aerosol layer.

This relationship highlights that the sub-inversion aerosol simultaneously enhances the local downward radiation and intensifies the radiative energy loss of the Arctic atmosphere to space.

4.3. Negative Radiative Forcing of Surface-Based Inversions

The radiative surface inversion exerts a dual influence on the longwave radiation balance. On the one hand, it increases the downward longwave flux, thereby slowing the radiative cooling of the surface. On the other hand, having a higher temperature than the underlying surface, the inversion layer becomes the main source of upward longwave emission, enhancing the energy loss of the troposphere through the infrared transparency windows.

In the 1980s, this “anti-greenhouse” effect was strongly amplified by the presence of aerosol-condensation layers, which increased the emissivity of the inversion layer. Under modern conditions, against the background of a sharp decline in aerosol concentrations, the temperature structure of the inversion is preserved, but its radiative impact is now limited exclusively to the selective emission of gases. Thus, the “cleansing” of the Arctic atmosphere from sulfate aerosol has weakened an important channel of efficient heat release into space, which represents a significant factor in the ongoing transformation of the region’s climate.

4.4. How Different Aerosol Sources Change Atmospheric Emissivity by Season

Satellite observations from TROPOMI [22], presented in Figure 10, illustrate the spatial distribution of the column-averaged carbon monoxide (XCO) and the Aerosol Index (AER) for August 2020 and 2021.

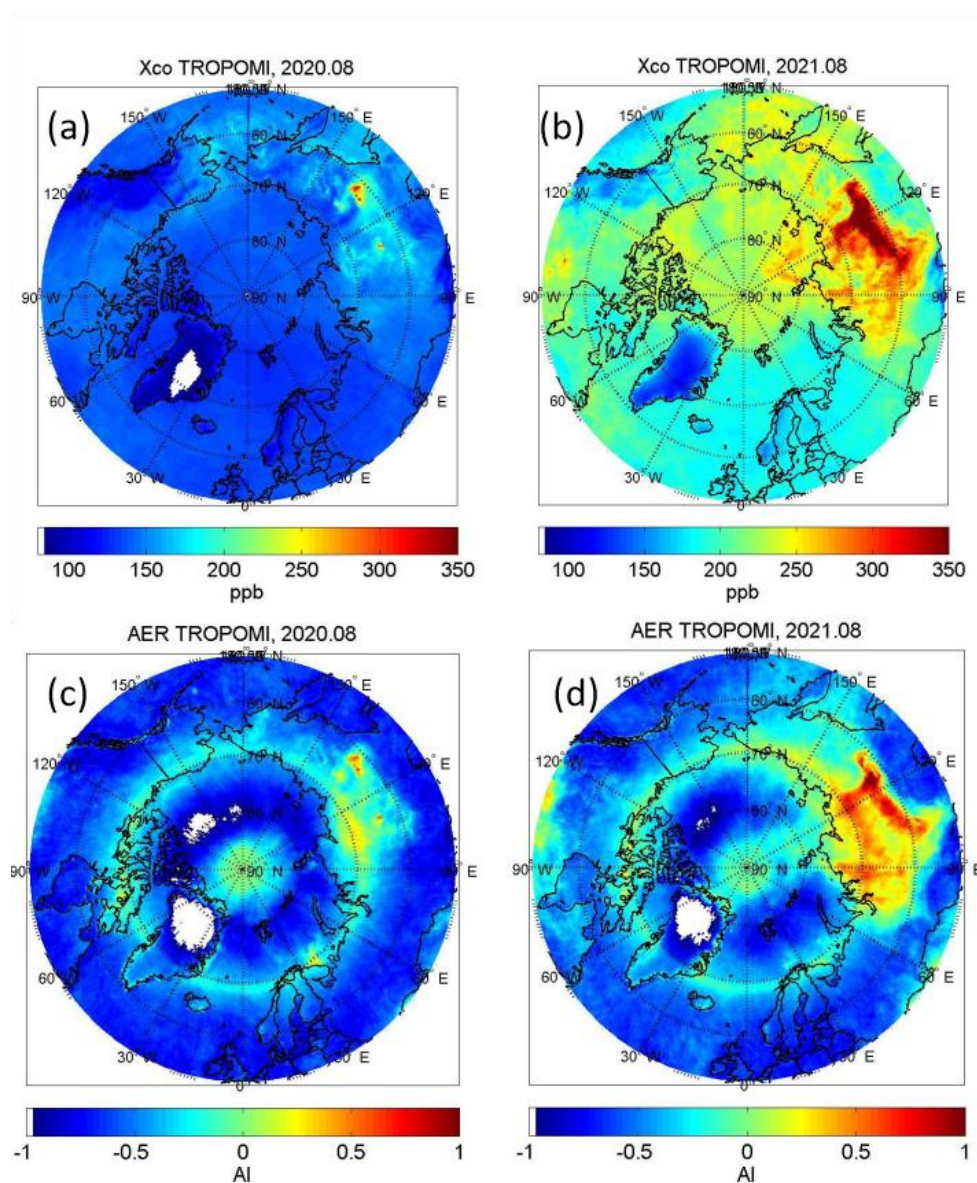


Figure 10. Data from TROPOMI/Sentinel-5 Precursor for August 2020 and 2021; a and b are monthly maps of CO concentrations averaged over the atmospheric total column. C and d are corresponding maps for the Aerosol Index.

In 2020, low XCO values and weak positive AER anomalies dominated the high latitudes, indicating a limited contribution of pyrogenic emissions to the formation of the summer aerosol maximum. In contrast, the situation in 2021 was markedly different: regions with elevated XCO and a strengthened aerosol signal reflected large-scale forest fires and the long-range transport of smoke into the Arctic. In this context, carbon monoxide serves as a reliable marker of pyrogenic activity, as its concentrations closely follow the smoke plumes.

Figure 10. TROPOMI/Sentinel-5 Precursor data for August 2020 and 2021. Panels (a) and (b) show monthly maps of CO concentrations averaged over the total atmospheric column; panels (c) and (d) present the corresponding maps of the Aerosol Index.

A comparison of Figure 10 with the two-peaked seasonal curve of atmospheric emissivity (Figure 7) shows that the summer maximum is driven by pyrogenic aerosols—soot and organic carbon. The spring maximum, by contrast, is formed by sulfate aerosol produced through the oxidation of sulfur dioxide transported from industrial regions of Eurasia. Observations from the

MOSAIC expedition confirm the dominance of sulfates in late winter and early spring, as well as the minimal abundance of absorbing particles during this period.

Seasonal variations in Arctic atmospheric emissivity are driven by aerosol types: spring sulfates and summer smoke. Here, CO levels serve as a measure of the radiative impact of wildfires on the region.

4.5. Radiation Regime of the Arctic in the Context of Declining Anthropogenic Emissions

The results obtained indicate that the Arctic has entered a new phase of its longwave radiation regime. Whereas in the 1980s the longwave fluxes were strongly modified by aerosol-condensation layers, their influence is now minimal. This transition implies a weakening of the near-surface “greenhouse” haze effect, a reduction in longwave absorption within the surface layer, and a diminished role of aerosol in shaping the regional energy balance. As a consequence, the relative importance of the gaseous atmosphere and the temperature structure of the surface inversion has increased. These changes must be taken into account when interpreting modern observations and developing climate models, as the disappearance of longwave-active aerosol alters the structure of the radiation budget and may influence the mechanisms of Arctic amplification.

5. Conclusions

The analysis of the long-term evolution of the longwave aerosol effect in the Arctic, based on a comparison of archival observations with modern measurements from the MOSAIC expedition, leads to several key conclusions.

First, the radiation regime of the Arctic has undergone a pronounced transformation over the past four decades. Whereas in the late twentieth century the sub-inversion haze acted as an important radiative agent, the near-zero modern values of the NLAE parameter indicate a transition toward a predominantly gas-controlled longwave regime.

Second, the observed decline in the aerosol effect is consistent with the global reduction in anthropogenic sulfur dioxide emissions. The decrease in sulfate aerosol concentrations in the Arctic troposphere [3] appears to have contributed to a reduction in the integral emissivity of the atmosphere during the winter–spring period.

Third, it has been shown that sub-inversion aerosol haze historically enhanced the longwave energy loss of the Earth–atmosphere system. By increasing the upward longwave flux through the infrared transparency windows, the aerosol layer acted as a mechanism of negative radiative feedback.

Finally, the “cleansing” of the Arctic atmosphere from sulfate aerosol—resulting from successful reductions in sulfur dioxide emissions—has led to a substantial weakening of this radiative heat-loss channel. This effect may paradoxically enhance Arctic warming, as the efficiency of longwave energy discharge into space has significantly decreased in recent decades.

These findings, supported by the spectral characteristics of outgoing radiation described in the classical works of Kondratyev (1980) [23], suggest that anthropogenic aerosol should be considered not only as a pollutant but also as an important historical regulator of the energy balance of the polar regions.

References

1. Shaw, G.E. The Arctic haze phenomenon. *Bull. Am. Meteorol. Soc.* 1995, 76, 2403–2414.
2. Yurganov, L.; Rakitin, V. Two decades of satellite observations of carbon monoxide confirm the increase in Northern Hemispheric wildfires. *Atmosphere* 2022, 13, 1479.
3. Zachek, A.S. The experimental investigation of the radiation effects of Arctic haze. *Trudy AARI; Gidrometeoizdat: St. Petersburg, Russia*, 1995. (In Russian)
4. Andreas, E.L.; Fairall, C.W.; Guest, P.S.; Persson, O. Ice Camp Surface Mesonet NCAR PAM III 5 Minute (FINAL), Version 1.0; Dataset, 2012. <https://doi.org/10.5065/D6RF5SD1>.

5. Pirazzini, R.; Hannula, H.-R.; Shupe, M.D.; Uttal, T.; Cox, C.J.; Costa, D.; Persson, P.O.G.; Brasseur, Z. Upward and downward broadband irradiance during MOSAiC; PANGAEA Dataset, 2022. <https://doi.org/10.1594/PANGAEA.952359>.
6. Wexler, H. Cooling in the lower atmosphere and the formation of polar air. *Mon. Weather Rev.* 1936, 64, 122–136.
7. Curry, J.A. On the formation of continental polar air. *J. Atmos. Sci.* 1983, 40, 2278–2292
8. Hobbs, W.R. Longwave Radiation and Arctic Haze: An Observational Study; Naval Postgraduate School: Monterey, CA, USA, 1988.
9. Overland, J.E.; Guest, P.S. The Arctic snow and air temperature budget over sea ice during winter; NOAA PMEL & Naval Postgraduate School: Seattle, WA, USA.
10. Makshtas, A.P.; Timachev, V.F.; Zachek, A.S. Processes of air–sea interaction in polar regions. In ACSYS Conference on the Dynamics of the Arctic Climate System; WMO/TD No. 760: Geneva, Switzerland, 1994.
11. Hinzpeter, H. Report on the comparisons of radiation balance meters carried out in the Meteorological Main Observatory Potsdam. *Z. Meteorol.* 1953, 7, 33–48.
12. Zachek, A.S. On the possibility of using a pyrgeometer with a new element base in the subsystem of ground-based actinometric observations in polar regions. In *Meteorological Research in Antarctica, 3rd All-Union Symposium*; Gidrometeoizdat: Leningrad, USSR, 1986; Part II. (In Russian)
13. Zachek, S.I. Instrument for measuring the longwave radiation balance. In *Actinometry, Atmospheric Optics, and Ozonometry*; Gidrometeoizdat: Leningrad, USSR, 1985; Issue 487, p. 42. (In Russian)
14. Kipp & Zonen. CGR4 and SGR4 Pyrgeometers Instruction Manual; OTT HydroMet: Delft, The Netherlands, 2021; 44p.
15. Gröbner, J.; Wacker, S. The World Infrared Standard Group (WISG): Calibration and stability. *AIP Conf. Proc.* 2021, 2353, 050004.
16. Riihelä, A.; et al. The Impact of Instrument Cleaning and Icing on Ground-Based Solar Radiation Measurements in the High Arctic. *Earth Space Sci.* 2020, 7, e2020EA001147.
17. König-Langlo, G.; Zachek, A. Radiation budget measurements over Antarctic sea ice in late winter. In *Sea Ice and Climate*; WCRP: Bremerhaven, Germany, 1990; pp. 41–44.
18. Zaitseva, N.A. Historical developments in radiosonde systems in the former Soviet Union. *Bull. Am. Meteorol. Soc.* 1993, 74, 1893–1900.
19. Zeng, Y.; Mech, M.; Ehrlich, A. Hygroscopic aerosols amplify longwave downward radiation in the Arctic. *Atmos. Chem. Phys.* 2025, 25, 3889–3907.
20. Shechter, E.M. Method for calculating longwave radiation fluxes in the atmosphere. *Trudy GGO* 1957, 67. (In Russian)
21. Crippa, M.; Guizzardi, D.; Pagani, F.; et al. EDGAR v8.0 Global Air Pollutant Emissions; European Commission, JRC, 2023.
22. European Space Agency (ESA), 2020–2021. Sentinel5P TROPOMI Level2 Products. Available at: <https://s5phub.copernicus.eu> (Accessed: of 21 February 2026)
23. Kondratyev, K.Ya. Radiative Factors of Modern Global Climate Changes; Gidrometeoizdat: Leningrad, USSR, 1980. (In Russian)

Disclaimer/Publisher’s Note: The statements, opinions and data contained in all publications are solely those of the individual author(s) and contributor(s) and not of MDPI and/or the editor(s). MDPI and/or the editor(s) disclaim responsibility for any injury to people or property resulting from any ideas, methods, instructions or products referred to in the content.